Anomalous Wtb coupling in hadronic collisions

Karol Kołodziej

Institute of Physics

University of Silesia, Katowice

LHCPhenoNet Mid-Term Meeting

Ravello, Italy, 16-20 September, 2012

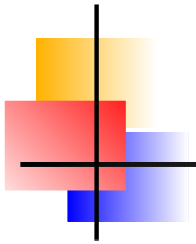

Outline

- Top quark production at hadron colliders.

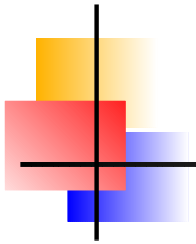

Outline

- Top quark production at hadron colliders.
- Anomalous Wtb coupling.

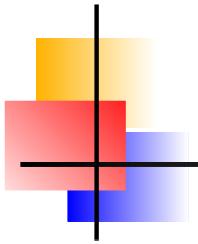

Outline

- Top quark production at hadron colliders.
- Anomalous Wtb coupling.
- Computation with `carlomat`.

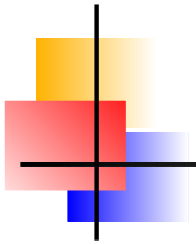

Outline

- Top quark production at hadron colliders.
- Anomalous Wtb coupling.
- Computation with `carlomat`.
- Sample results.

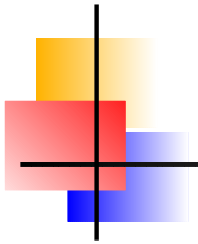

Outline

- Top quark production at hadron colliders.
- Anomalous Wtb coupling.
- Computation with `carlomat`.
- Sample results.
- Summary and outlook.

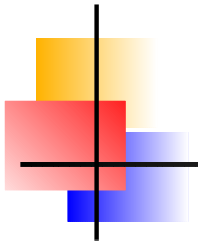

Motivation

The top quark is the heaviest particle ever observed, with mass close to the energy scale of the electroweak symmetry breaking.

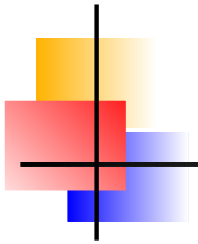

Motivation

The top quark is the heaviest particle ever observed, with mass close to the energy scale of the electroweak symmetry breaking.

$\Rightarrow$ The top quark physics is an ideal place to look for non-standard effects which may reveal themselves through departures of the top quark properties and interactions from those predicted by the SM.

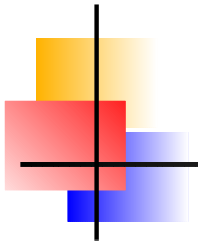

Motivation

The top quark is the heaviest particle ever observed, with mass close to the energy scale of the electroweak symmetry breaking.

$\Rightarrow$ The top quark physics is an ideal place to look for non-standard effects which may reveal themselves through departures of the top quark properties and interactions from those predicted by the SM.

The observation of a forward-backward asymmetry (FBA) in the top quark pair production in high energy proton-antiproton collisions at Tevatron that exceeds the SM expectation is an indication that this conjecture may be true.

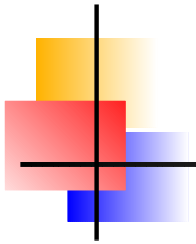

Top quark production at hadron colliders

The top quarks are produced dominantly in pairs through

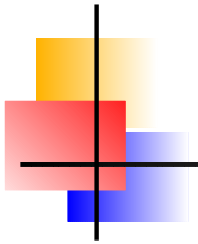

Top quark production at hadron colliders

The top quarks are produced dominantly in pairs through the quark-antiquark annihilation process

$$q\bar{q} \rightarrow t\bar{t}, \qquad \text{(dominates at the Tevatron)},$$

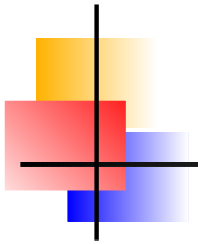

Top quark production at hadron colliders

The top quarks are produced dominantly in pairs through the quark-antiquark annihilation process

$$q\bar{q} \rightarrow t\bar{t}, \qquad \text{(dominates at the Tevatron)},$$

or the gluon-gluon fusion process

$$gg \rightarrow t\bar{t}, \qquad \text{(dominates at the LHC)}.$$

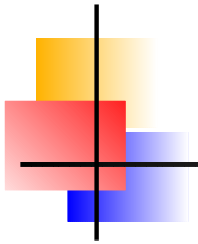

Top quark production at hadron colliders

The top quarks are produced dominantly in pairs through the quark-antiquark annihilation process

$$q\bar{q} \to t\bar{t}, \qquad \text{(dominates at the Tevatron)},$$

or the gluon-gluon fusion process

$$gg \to t\bar{t}, \qquad \text{(dominates at the LHC)}.$$

Single top production processes, as e.g.

$$qb \to q't, \quad q\bar{q}' \to t\bar{b}, \quad \text{or} \quad qg \to q't\bar{b},$$

have much smaller cross sections.

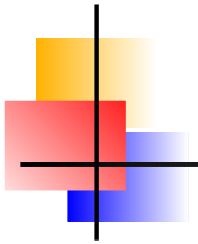

Top quark production at hadron colliders

The top quarks are produced dominantly in pairs through the quark-antiquark annihilation process

$$q\bar{q} \to t\bar{t}, \qquad \text{(dominates at the Tevatron)},$$

or the gluon-gluon fusion process

$$gg \to t\bar{t}, \qquad \text{(dominates at the LHC)}.$$

Single top production processes, as e.g.

$$qb \to q't, \quad q\bar{q}' \to t\bar{b}, \quad \text{or} \quad qg \to q't\bar{b},$$

have much smaller cross sections.

$\Rightarrow$ They are not addressed in this talk but may be treated exactly on the same footing.

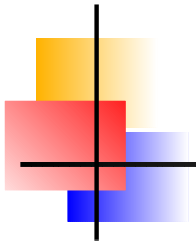

Top quark pair production at hadron colliders

- As the top and antitop decay before they hadronize, almost exclusively into bW^+ and $\bar{b}W^-$

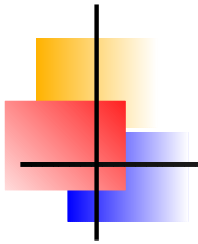

Top quark pair production at hadron colliders

- As the top and antitop decay before they hadronize, almost exclusively into bW^+ and $\bar{b}W^-$
- and W's decay into $f\bar{f}'$-pairs,

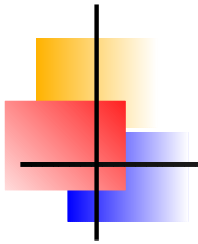

Top quark pair production at hadron colliders

- As the top and antitop decay before they hadronize, almost exclusively into bW^+ and $\bar{b}W^-$
- and W's decay into $f\bar{f}'$-pairs,

the hard scattering processes of the form

$$q\bar{q}\,(gg) \;\to\; bf_1\bar{f}'_1\bar{b}f_2\bar{f}'_2,$$

where $f_1, f'_2 = \nu_e, \nu_\mu, \nu_\tau, u, c$ and $f'_1, f_2 = e^-, \mu^-, \tau^-, d, s$, should be considered with a complete set of the Feynman diagrams.

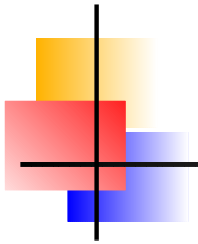

Top quark pair production at hadron colliders

- As the top and antitop decay before they hadronize, almost exclusively into bW^+ and $\bar{b}W^-$
- and W's decay into $f\bar{f}'$-pairs,

the hard scattering processes of the form

$$q\bar{q}\,(gg) \;\rightarrow\; bf_1\bar{f}'_1\bar{b}f_2\bar{f}'_2,$$

where $f_1, f'_2 = \nu_e, \nu_\mu, \nu_\tau, u, c$ and $f'_1, f_2 = e^-, \mu^-, \tau^-, d, s$, should be considered with a complete set of the Feynman diagrams.

The top quark production is measured in channels where at least one W decays leptonically.

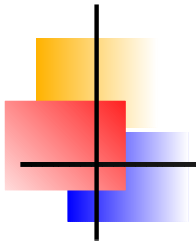

Top quark pair production at hadron colliders

There are 718 Feynman diagrams of the reaction

$$u\bar{u} \to bud\bar{b}\mu^{-}\bar{\nu}_{\mu},$$

in the unitary gauge, neglecting masses lighter than m_b and CKM mixing.

Top quark pair production at hadron colliders

There are 718 Feynman diagrams of the reaction

$$u\bar{u} \to bud\bar{b}\mu^-\bar{\nu}_\mu,$$

in the unitary gauge, neglecting masses lighter than m_b and CKM mixing. Some examples:

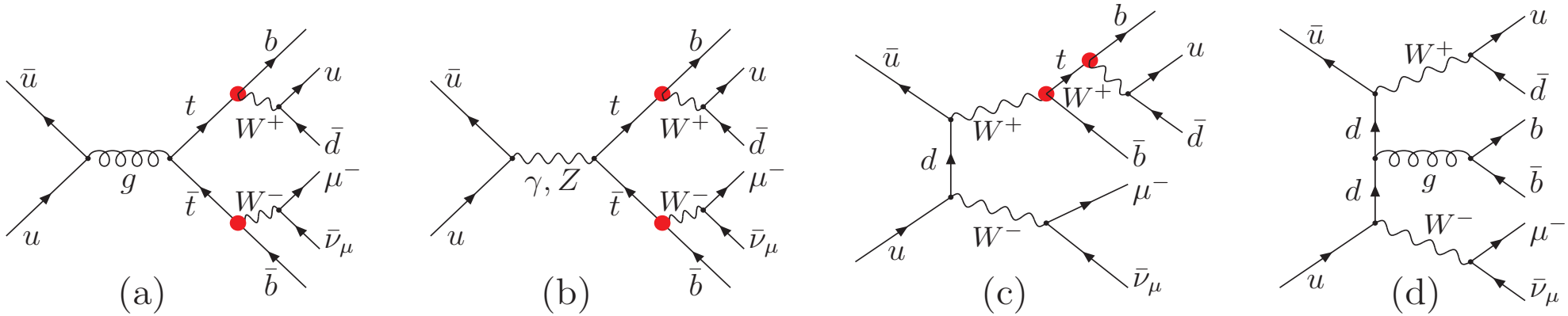

(a) and (b) 'signal', (c) and (d) 'background'.

There are two Wtb couplings for each $t\bar{t}$ production signal diagram and the single top production diagram.

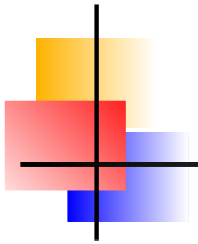

Anomalous Wtb coupling

The presence of an anomalous Wtb coupling influences the top quark pair production in two basic ways.

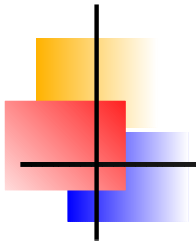

Anomalous Wtb coupling

The presence of an anomalous Wtb coupling influences the top quark pair production in two basic ways.

- It changes the total decay width of the top quark, which substantially alters the total cross sections.

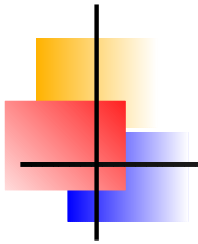

Anomalous Wtb coupling

The presence of an anomalous Wtb coupling influences the top quark pair production in two basic ways.

- It changes the total decay width of the top quark, which substantially alters the total cross sections.
- It may change differential distributions of the final state particles, in particular angular distributions of the final state lepton.

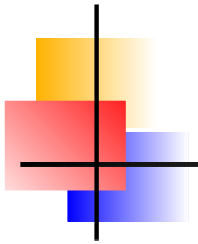

Anomalous Wtb coupling

The presence of an anomalous Wtb coupling influences the top quark pair production in two basic ways.

- It changes the total decay width of the top quark, which substantially alters the total cross sections.
- It may change differential distributions of the final state particles, in particular angular distributions of the final state lepton.

The latter allow to determine e.g. the polarization of the W-bosons produced in top-quark decays, or the top quark polarization itself.

Anomalous Wtb coupling

The most general effective Lagrangian of the Wtb interaction containing operators of dimension four and five:

$$L_{Wtb} = \frac{g}{\sqrt{2}} V_{tb} \left[W_\mu^- \bar{b} \gamma^\mu \left(f_1^L P_L + f_1^R P_R \right) t \right.$$

$$+ \frac{g}{\sqrt{2}} V_{tb}^* \left[W_\mu^+ \bar{t} \gamma^\mu \left(\bar{f}_1^L P_L + \bar{f}_1^R P_R \right) b \right.$$

Anomalous Wtb coupling

The most general effective Lagrangian of the Wtb interaction containing operators of dimension four and five:

$$
\begin{aligned}
L_{Wtb} &= \frac{g}{\sqrt{2}} V_{tb} \left[W_\mu^- \bar{b} \gamma^\mu \left(f_1^L P_L + f_1^R P_R \right) t \right. \\
&\qquad \left. - \frac{1}{m_W} \partial_\nu W_\mu^- \bar{b} \sigma^{\mu\nu} \left(f_2^L P_L + f_2^R P_R \right) t \right] \\
&+ \frac{g}{\sqrt{2}} V_{tb}^* \left[W_\mu^+ \bar{t} \gamma^\mu \left(\bar{f}_1^L P_L + \bar{f}_1^R P_R \right) b \right. \\
&\qquad \left. - \frac{1}{m_W} \partial_\nu W_\mu^+ \bar{t} \sigma^{\mu\nu} \left(\bar{f}_2^L P_L + \bar{f}_2^R P_R \right) b \right] .
\end{aligned}
$$

Anomalous Wtb coupling

The most general effective Lagrangian of the Wtb interaction containing operators of dimension four and five:

$$\begin{aligned} L_{Wtb} &= \frac{g}{\sqrt{2}} V_{tb} \left[W_\mu^- \bar{b} \gamma^\mu \left(f_1^L P_L + f_1^R P_R \right) t \right. \\ &\qquad \left. - \frac{1}{m_W} \partial_\nu W_\mu^- \bar{b} \sigma^{\mu\nu} \left(f_2^L P_L + f_2^R P_R \right) t \right] \\ &+ \frac{g}{\sqrt{2}} V_{tb}^* \left[W_\mu^+ \bar{t} \gamma^\mu \left(\bar{f}_1^L P_L + \bar{f}_1^R P_R \right) b \right. \\ &\qquad \left. - \frac{1}{m_W} \partial_\nu W_\mu^+ \bar{t} \sigma^{\mu\nu} \left(\bar{f}_2^L P_L + \bar{f}_2^R P_R \right) b \right] . \end{aligned}$$

Other dimension five terms that are possible for off shell W bosons vanish if the W's decay into mass-less fermions.

Anomalous Wtb coupling

$$
\begin{aligned}
L_{Wtb} &= \frac{g}{\sqrt{2}} V_{tb} \left[W_\mu^- \bar{b} \gamma^\mu \left(f_1^L P_L + f_1^R P_R \right) t \right. \\
&\qquad \left. - \frac{1}{m_W} \partial_\nu W_\mu^- \bar{b} \sigma^{\mu\nu} \left(f_2^L P_L + f_2^R P_R \right) t \right] \\
&+ \frac{g}{\sqrt{2}} V_{tb}^* \left[W_\mu^+ \bar{t} \gamma^\mu \left(\bar{f}_1^L P_L + \bar{f}_1^R P_R \right) b \right. \\
&\qquad \left. - \frac{1}{m_W} \partial_\nu W_\mu^+ \bar{t} \sigma^{\mu\nu} \left(\bar{f}_2^L P_L + \bar{f}_2^R P_R \right) b \right] .
\end{aligned}
$$

The lowest order SM Lagrangian of the Wtb interaction is reproduced by setting:

$$
f_1^L = \bar{f}_1^L = 1, \qquad f_1^R = f_2^R = f_2^L = \bar{f}_1^R = \bar{f}_2^R = \bar{f}_2^L = 0.
$$

Anomalous Wtb coupling

$$
\begin{aligned}
L_{Wtb} &= \frac{g}{\sqrt{2}} V_{tb} \left[W_\mu^- \bar{b} \gamma^\mu \left(f_1^L P_L + f_1^R P_R \right) t \right. \\
&\qquad \left. - \frac{1}{m_W} \partial_\nu W_\mu^- \bar{b} \sigma^{\mu\nu} \left(f_2^L P_L + f_2^R P_R \right) t \right] \\
&+ \frac{g}{\sqrt{2}} V_{tb}^* \left[W_\mu^+ \bar{t} \gamma^\mu \left(\bar{f}_1^L P_L + \bar{f}_1^R P_R \right) b \right. \\
&\qquad \left. - \frac{1}{m_W} \partial_\nu W_\mu^+ \bar{t} \sigma^{\mu\nu} \left(\bar{f}_2^L P_L + \bar{f}_2^R P_R \right) b \right] .
\end{aligned}
$$

If CP is conserved then the following relationships hold

Anomalous Wtb coupling

$$
\begin{aligned}
L_{Wtb} &= \frac{g}{\sqrt{2}} V_{tb} \left[W_\mu^- \bar{b} \gamma^\mu \left(f_1^L P_L + f_1^R P_R \right) t \right. \\
&\qquad \left. - \frac{1}{m_W} \partial_\nu W_\mu^- \bar{b} \sigma^{\mu\nu} \left(f_2^L P_L + f_2^R P_R \right) t \right] \\
&+ \frac{g}{\sqrt{2}} V_{tb}^* \left[W_\mu^+ \bar{t} \gamma^\mu \left(\bar{f}_1^L P_L + \bar{f}_1^R P_R \right) b \right. \\
&\qquad \left. - \frac{1}{m_W} \partial_\nu W_\mu^+ \bar{t} \sigma^{\mu\nu} \left(\bar{f}_2^L P_L + \bar{f}_2^R P_R \right) b \right] .
\end{aligned}
$$

If CP is conserved then the following relationships hold

$$
\bar{f}_1^{R\,*} = f_1^R, \quad \bar{f}_1^{L\,*} = f_1^L, \qquad \text{and} \qquad \bar{f}_2^{R\,*} = f_2^L, \quad \bar{f}_2^{L\,*} = f_2^R .
$$

Anomalous Wtb coupling

$$
\begin{aligned}
L_{Wtb} &= \frac{g}{\sqrt{2}} V_{tb} \left[W_\mu^- \bar{b} \gamma^\mu \left(f_1^L P_L + f_1^R P_R \right) t \right. \\
&\qquad \left. - \frac{1}{m_W} \partial_\nu W_\mu^- \bar{b} \sigma^{\mu\nu} \left(f_2^L P_L + f_2^R P_R \right) t \right] \\
&+ \frac{g}{\sqrt{2}} V_{tb}^* \left[W_\mu^+ \bar{t} \gamma^\mu \left(\bar{f}_1^L P_L + \bar{f}_1^R P_R \right) b \right. \\
&\qquad \left. - \frac{1}{m_W} \partial_\nu W_\mu^+ \bar{t} \sigma^{\mu\nu} \left(\bar{f}_2^L P_L + \bar{f}_2^R P_R \right) b \right] .
\end{aligned}
$$

If CP is conserved then the following relationships hold

$$
\bar{f}_1^{R\,*} = f_1^R, \quad \bar{f}_1^{L\,*} = f_1^L, \qquad \text{and} \qquad \bar{f}_2^{R\,*} = f_2^L, \quad \bar{f}_2^{L\,*} = f_2^R .
$$

$\Rightarrow$ 4 independent form factors are left.

Anomalous Wtb coupling

The Feynman rules resulting from the Lagrangian

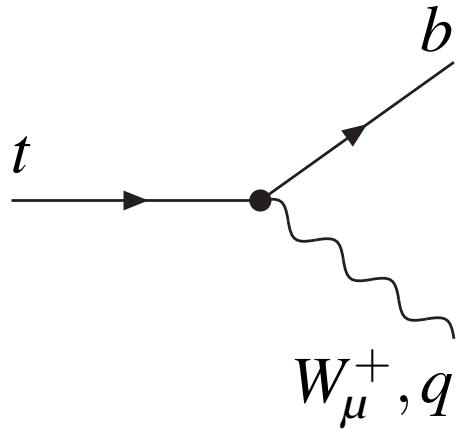

$$\longrightarrow \quad \Gamma^{\mu}_{t\to bW^+} = \frac{g}{\sqrt{2}} V_{tb} \left[\gamma^\mu \left(f_1^L P_L + f_1^R P_R \right) - i \frac{q_\nu}{m_W} \sigma^{\mu\nu} \left(f_2^L P_L + f_2^R P_R \right) \right],$$

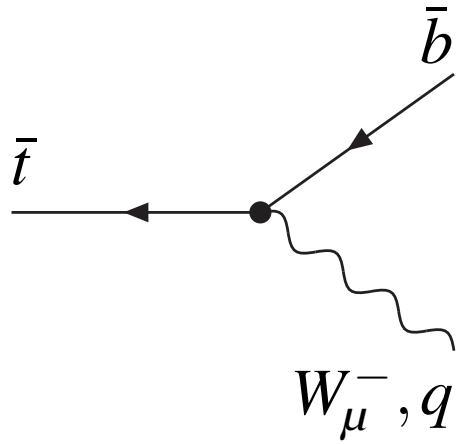

$$\longrightarrow \quad \Gamma^{\mu}_{\bar{t}\to \bar{b}W^-} = \frac{g}{\sqrt{2}} V_{tb}^* \left[\gamma^\mu \left(\bar{f}_1^L P_L + \bar{f}_1^R P_R \right) - i \frac{q_\nu}{m_W} \sigma^{\mu\nu} \left(\bar{f}_2^L P_L + \bar{f}_2^R P_R \right) \right],$$

q is a four momentum of the W boson outgoing from the vertex.

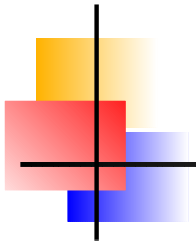

Anomalous Wtb coupling

Direct Tevatron limits, obtained by investigating two form factors at a time and assuming the other two at their SM values:

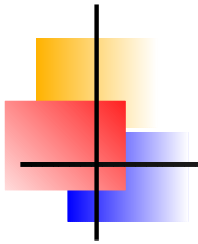

Anomalous Wtb coupling

Direct Tevatron limits, obtained by investigating two form factors at a time and assuming the other two at their SM values:

$$\left|V_{tb}\, f_1^R\right|^2 < 0.93, \qquad \left|V_{tb}\, f_2^R\right|^2 < 0.13, \qquad \left|V_{tb}\, f_2^L\right|^2 < 0.06.$$

[D0 Collaboration, Phys. Lett. B 708 (2012) 21.]

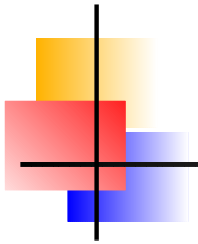

Anomalous Wtb coupling

Direct Tevatron limits, obtained by investigating two form factors at a time and assuming the other two at their SM values:

$$\left|V_{tb}\, f_1^R\right|^2 < 0.93, \qquad \left|V_{tb}\, f_2^R\right|^2 < 0.13, \qquad \left|V_{tb}\, f_2^L\right|^2 < 0.06.$$

[D0 Collaboration, Phys. Lett. B 708 (2012) 21.]

ATLAS limits, with one non-zero coupling at a time, $(V_{tb} \simeq 1)$:

$$\mathrm{Re}\, f_1^R \in [-0.20, 0.23], \quad \mathrm{Re}\, f_2^R \in [-0.08, 0.04], \quad \mathrm{Re}\, f_2^L \in [-0.14, 0.11].$$

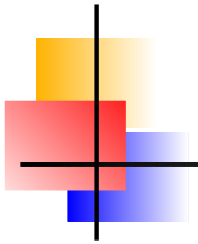

Anomalous Wtb coupling

Direct Tevatron limits, obtained by investigating two form factors at a time and assuming the other two at their SM values:

$$\left|V_{tb}\, f_1^R\right|^2 < 0.93, \qquad \left|V_{tb}\, f_2^R\right|^2 < 0.13, \qquad \left|V_{tb}\, f_2^L\right|^2 < 0.06.$$

[D0 Collaboration, Phys. Lett. B 708 (2012) 21.]
ATLAS limits, with one non-zero coupling at a time, $(V_{tb} \simeq 1)$:

$$\mathrm{Re}\, f_1^R \in [-0.20, 0.23], \quad \mathrm{Re}\, f_2^R \in [-0.08, 0.04], \quad \mathrm{Re}\, f_2^L \in [-0.14, 0.11].$$

Limits become weaker if two couplings are varied at a time (CMS).

Anomalous Wtb coupling

Direct Tevatron limits, obtained by investigating two form factors at a time and assuming the other two at their SM values:

$$\left|V_{tb}\, f_1^R\right|^2 < 0.93, \qquad \left|V_{tb}\, f_2^R\right|^2 < 0.13, \qquad \left|V_{tb}\, f_2^L\right|^2 < 0.06.$$

[D0 Collaboration, Phys. Lett. B 708 (2012) 21.]
ATLAS limits, with one non-zero coupling at a time, $(V_{tb} \simeq 1)$:

$$\mathrm{Re}\, f_1^R \in [-0.20, 0.23], \quad \mathrm{Re}\, f_2^R \in [-0.08, 0.04], \quad \mathrm{Re}\, f_2^L \in [-0.14, 0.11].$$

Limits become weaker if two couplings are varied at a time (CMS).
If CP is conserved then the right-handed vector coupling and tensor couplings can be indirectly constrained from $b \to s\gamma$ branching fraction.

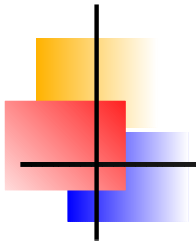

Computation

Many partonic sub-processes and large number of Feynman diagrams $\Rightarrow$ cross sections must be computed in a fully automatic way.

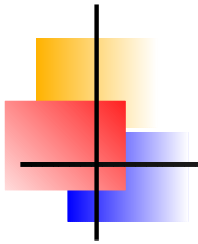

Computation

Many partonic sub-processes and large number of Feynman diagrams $\Rightarrow$ cross sections must be computed in a fully automatic way.

There are several multipurpose Monte Carlo generators as `HELAC/PHEGAS`, `AMAGIC++/Sherpa`, `O'Mega/Whizard`, `MadGraph/MadEvent`, `ALPGEN`, `CompHEP/CalcHEP`.

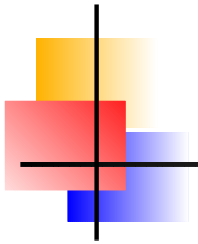

Computation

Many partonic sub-processes and large number of Feynman diagrams $\Rightarrow$ cross sections must be computed in a fully automatic way.

There are several multipurpose Monte Carlo generators as `HELAC/PHEGAS`, `AMAGIC++/Sherpa`, `O'Mega/Whizard`, `MadGraph/MadEvent`, `ALPGEN`, `CompHEP/CalcHEP`.

We will use other multi purpose MC program `carlomat`.

K. Kołodziej, Comput. Phys. Commun. **180** (2009) 1671.

Program is available from the CPC Program Library, or from `http://kk.us.edu.pl`.

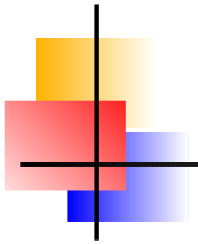

Computation

Many partonic sub-processes and large number of Feynman diagrams $\Rightarrow$ cross sections must be computed in a fully automatic way.

There are several multipurpose Monte Carlo generators as `HELAC/PHEGAS`, `AMAGIC++/Sherpa`, `O'Mega/Whizard`, `MadGraph/MadEvent`, `ALPGEN`, `CompHEP/CalcHEP`.

We will use other multi purpose MC program `carlomat`.

K. Kołodziej, Comput. Phys. Commun. **180** (2009) 1671.

Program is available from the CPC Program Library, or from `http://kk.us.edu.pl`.

Current version of `carlomat` has been supplemented with a few new subroutines necessary for calculation of the helicity amplitudes of the tensor couplings.

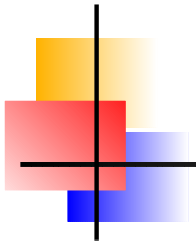

FBA in $t\bar{t}$ production at Tevatron

The $t\bar{t}$ invariant mass dependent forward-backward asymmetry is defined by

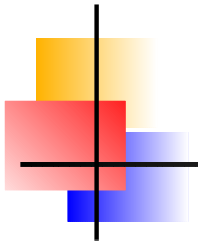

FBA in $t\bar{t}$ production at Tevatron

The $t\bar{t}$ invariant mass dependent forward-backward asymmetry is defined by

$$A_{t\bar{t}}(m_{t\bar{t},i}) = \frac{\sigma(\Delta y > 0, m_{t\bar{t},i}) - \sigma(\Delta y > 0, m_{t\bar{t},i})}{\sigma(\Delta y > 0, m_{t\bar{t},i}) + \sigma(\Delta y > 0, m_{t\bar{t},i})},$$

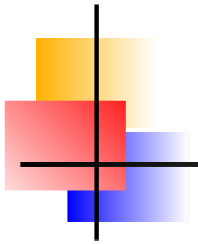

FBA in $t\bar{t}$ production at Tevatron

The $t\bar{t}$ invariant mass dependent forward-backward asymmetry is defined by

$$A_{t\bar{t}}(m_{t\bar{t},i}) = \frac{\sigma(\Delta y > 0, m_{t\bar{t},i}) - \sigma(\Delta y > 0, m_{t\bar{t},i})}{\sigma(\Delta y > 0, m_{t\bar{t},i}) + \sigma(\Delta y > 0, m_{t\bar{t},i})},$$

with $\Delta y = y_t - y_{\bar{t}}$ being a difference of rapidities of the t and $\bar{t}$ quarks with the invariant mass within i-th bin.

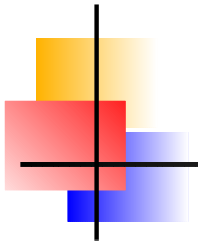

FBA in $t\bar{t}$ production at Tevatron

The $t\bar{t}$ invariant mass dependent forward-backward asymmetry is defined by

$$A_{t\bar{t}}(m_{t\bar{t},i}) = \frac{\sigma(\Delta y > 0, m_{t\bar{t},i}) - \sigma(\Delta y > 0, m_{t\bar{t},i})}{\sigma(\Delta y > 0, m_{t\bar{t},i}) + \sigma(\Delta y > 0, m_{t\bar{t},i})},$$

with $\Delta y = y_t - y_{\bar{t}}$ being a difference of rapidities of the t and $\bar{t}$ quarks with the invariant mass within i-th bin.

The total asymmetry is zero at the lowest order of SM, as quark pair production is symmetric under charge conjugation.

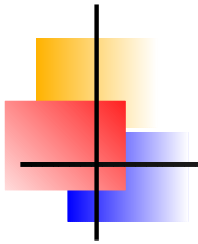

FBA in $t\bar{t}$ production at Tevatron

The $t\bar{t}$ invariant mass dependent forward-backward asymmetry is defined by

$$A_{t\bar{t}}(m_{t\bar{t},i}) = \frac{\sigma(\Delta y > 0, m_{t\bar{t},i}) - \sigma(\Delta y > 0, m_{t\bar{t},i})}{\sigma(\Delta y > 0, m_{t\bar{t},i}) + \sigma(\Delta y > 0, m_{t\bar{t},i})},$$

with $\Delta y = y_t - y_{\bar{t}}$ being a difference of rapidities of the t and $\bar{t}$ quarks with the invariant mass within i-th bin.

The total asymmetry is zero at the lowest order of SM, as quark pair production is symmetric under charge conjugation.

At NLO the interference of processes that differ under charge conjugation leads to a small forward-backward asymmetry of 0.06 ± 0.01.

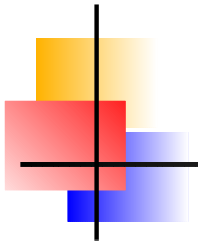

FBA in $t\bar{t}$ production at Tevatron

Both CDF and D0 measured higher values of the FBA at a parton level, but the results are still consistent with SM.

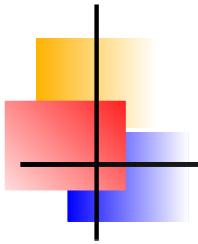

FBA in $t\bar{t}$ production at Tevatron

Both CDF and D0 measured higher values of the FBA at a parton level, but the results are still consistent with SM.

However, CDF measured:

$$A_{t\bar{t}}(m_{t\bar{t}} \geq 450\,\mathrm{GeV}/c^2) = 0.475 \pm 0.114$$

to be compared with the NLO prediction of 0.088 ± 0.013.

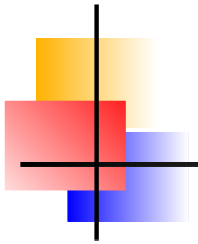

FBA in $t\bar{t}$ production at Tevatron

Both CDF and D0 measured higher values of the FBA at a parton level, but the results are still consistent with SM.
However, CDF measured:

$$A_{t\bar{t}}(m_{t\bar{t}} \geq 450\,\mathrm{GeV}/c^2) = 0.475 \pm 0.114$$

to be compared with the NLO prediction of 0.088 ± 0.013.
The higher order QCD [Ahrens et al.; Kidonakis] and electroweak [Hollik, Pagani; Kühn, Rodrigo] corrections increase the FBA in the high $m_{t\bar{t}}$, but a 3σ deviation between the measurement and the SM prediction still remains.

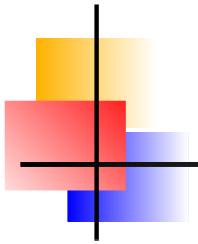

FBA in $t\bar{t}$ production at Tevatron

Both CDF and D0 measured higher values of the FBA at a parton level, but the results are still consistent with SM.
However, CDF measured:

$$A_{t\bar{t}}(m_{t\bar{t}} \geq 450\,\mathrm{GeV}/c^2) = 0.475 \pm 0.114$$

to be compared with the NLO prediction of 0.088 ± 0.013.
The higher order QCD [Ahrens et al.; Kidonakis] and electroweak [Hollik, Pagani; Kühn, Rodrigo] corrections increase the FBA in the high $m_{t\bar{t}}$, but a 3σ deviation between the measurement and the SM prediction still remains.

Different new physics mechanisms including axigluons, diquarks, new weak bosons, extra-dimensions, etc. have been used to explain the asymmetry.

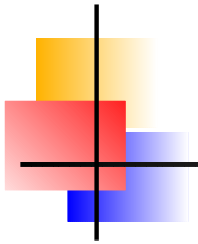

FBA in $t\bar{t}$ production at Tevatron

Let's see if the anomalous Wtb coupling can generate nonzero value of $A_{t\bar{t}}$ in the leading order by modifying the top quark decays with respect to SM.

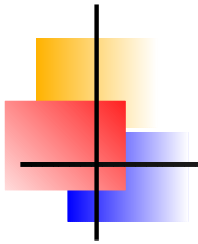

FBA in $t\bar{t}$ production at Tevatron

Let's see if the anomalous Wtb coupling can generate nonzero value of $A_{t\bar{t}}$ in the leading order by modifying the top quark decays with respect to SM.
Calculate the cross section of

$$p\bar{p} \to t\bar{t}$$

with `carlomat` taking into account all hard scattering sub-processes of $q\bar{q}$ annihilation into 6 fermion final states corresponding to one top quark decaying semileptonically $(t \to bl\nu_l)$ and the other hadronically $(t \to bq\bar{q}')$.

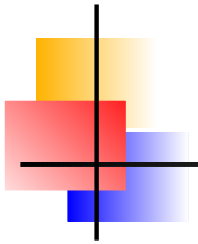

FBA in $t\bar{t}$ production at Tevatron

The $t\bar{t}$ production events are identified with the following acceptance cuts:

$$p_{Tl} > 50\,\mathrm{GeV}/c, \quad p_{Tj} > 50\,\mathrm{GeV}/c, \quad |\eta_l| < 2.0, \quad |\eta_j| < 2.5,$$

$$\not{E}^T > 20\,\mathrm{GeV}, \quad \Delta R_{ll,lj,jj} > 0.4,$$

where $\Delta R_{ik} = \sqrt{(\eta_i - \eta_k)^2 + (\varphi_i - \varphi_k)^2}$ is the separation in the pseudorapidity (η) –azimuthal angle (φ) plane between the objects i and k.

FBA in $t\bar{t}$ production at Tevatron

The $t\bar{t}$ production events are identified with the following acceptance cuts:

$$p_{Tl} > 50\,\mathrm{GeV}/c, \quad p_{Tj} > 50\,\mathrm{GeV}/c, \qquad |\eta_l| < 2.0, \quad |\eta_j| < 2.5,$$

$$\not{E}^T > 20\,\mathrm{GeV}, \qquad \Delta R_{ll,lj,jj} > 0.4,$$

where $\Delta R_{ik} = \sqrt{(\eta_i - \eta_k)^2 + (\varphi_i - \varphi_k)^2}$ is the separation in the pseudorapidity (η) –azimuthal angle (φ) plane between the objects i and k.

CTEQ6L parton distribution functions are used.

FBA in $t\bar{t}$ production at Tevatron

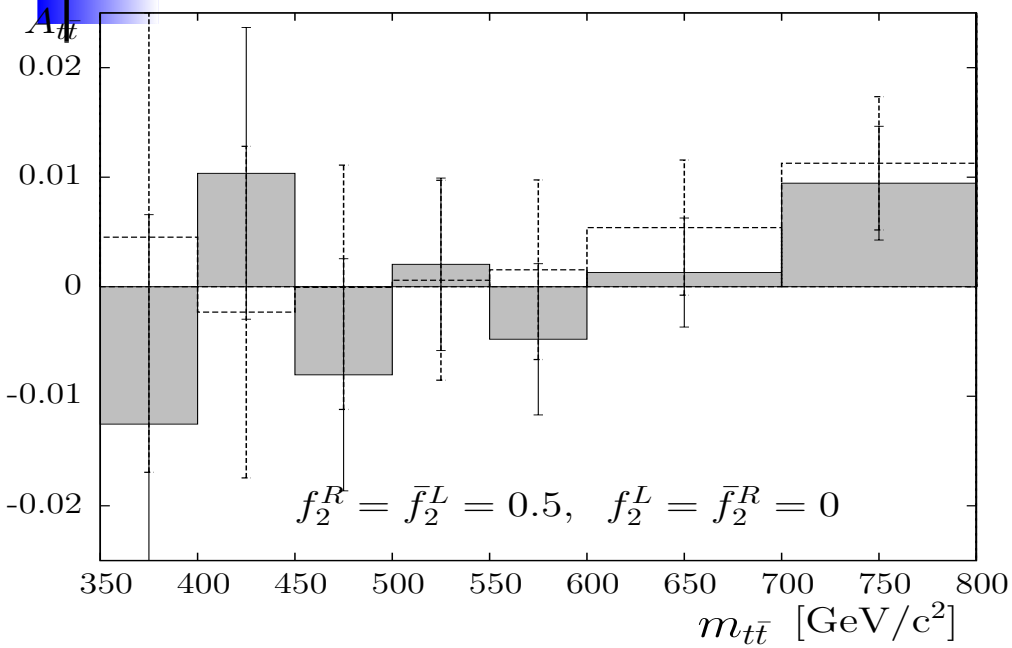

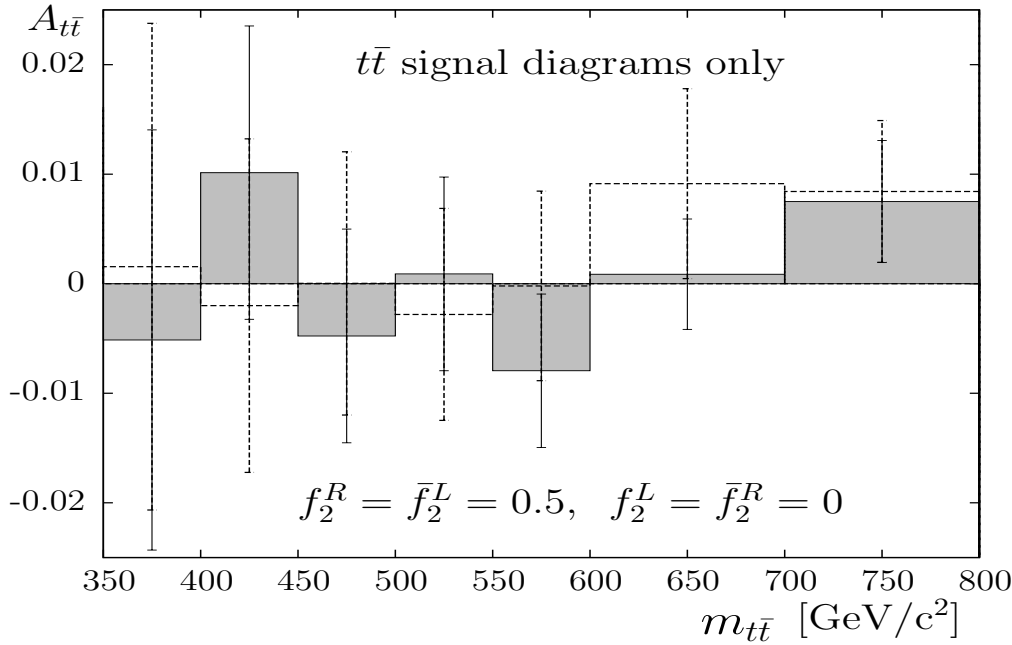

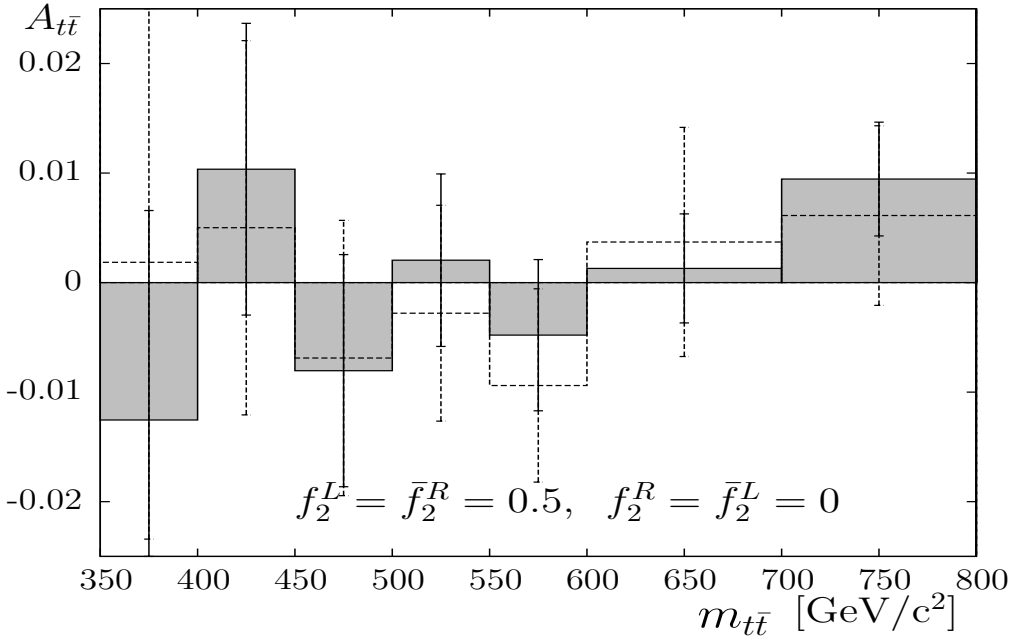

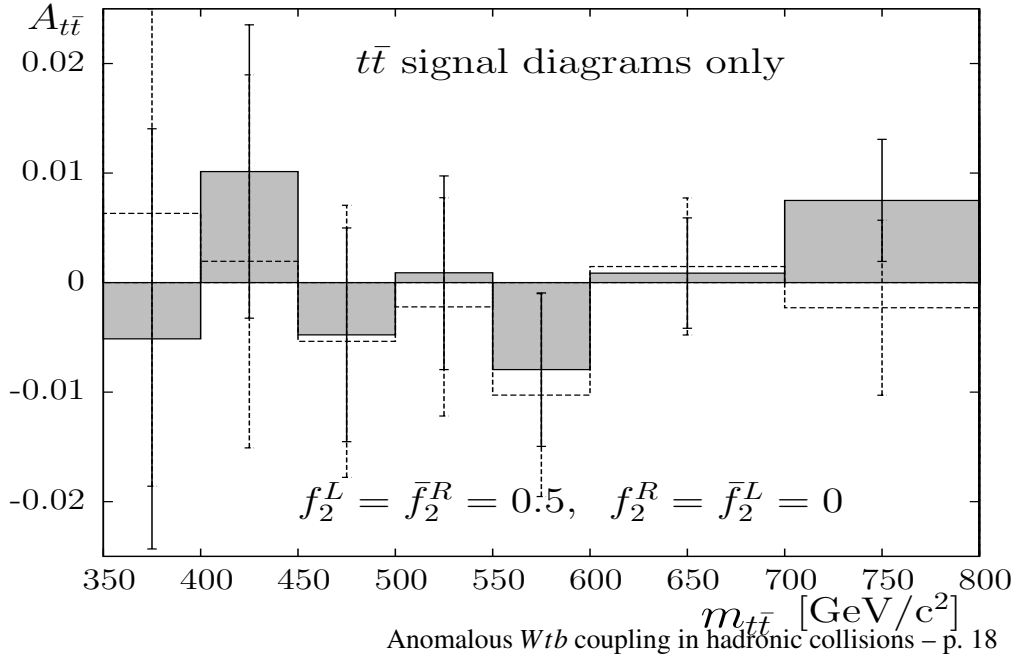

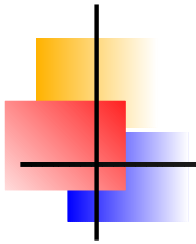

FBA in $t\bar{t}$ production at Tevatron

There are fluctuations in separate bins $\sim 1\sigma$, but integrated lowest order SM asymmetry is consistent with zero:

$$\begin{aligned} A_{t\bar{t}}^{\text{total}} &= -0.0013 \pm 0.0052, \\ A_{t\bar{t}}(m_{t\bar{t}} < 450\ \text{GeV}/c^2) &= 0.0009 \pm 0.0011 \\ A_{t\bar{t}}(m_{t\bar{t}} \geq 450\ \text{GeV}/c^2) &= -0.0027 \pm 0.0045. \end{aligned}$$

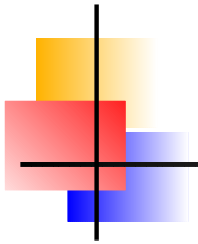

FBA in $t\bar{t}$ production at Tevatron

There are fluctuations in separate bins $\sim 1\sigma$, but integrated lowest order SM asymmetry is consistent with zero:

$$\begin{aligned} A_{t\bar{t}}^{\text{total}} &= -0.0013 \pm 0.0052, \\ A_{t\bar{t}}(m_{t\bar{t}} < 450\ \text{GeV}/c^2) &= 0.0009 \pm 0.0011 \\ A_{t\bar{t}}(m_{t\bar{t}} \geq 450\ \text{GeV}/c^2) &= -0.0027 \pm 0.0045. \end{aligned}$$

The presence of non zero tensor Wtb form factors does not change this in practice.

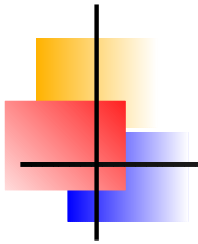

FBA in $t\bar{t}$ production at Tevatron

There are fluctuations in separate bins $\sim 1\sigma$, but integrated lowest order SM asymmetry is consistent with zero:

$$\begin{aligned} A_{t\bar{t}}^{\text{total}} &= -0.0013 \pm 0.0052, \\ A_{t\bar{t}}(m_{t\bar{t}} < 450\ \text{GeV}/c^2) &= 0.0009 \pm 0.0011 \\ A_{t\bar{t}}(m_{t\bar{t}} \geq 450\ \text{GeV}/c^2) &= -0.0027 \pm 0.0045. \end{aligned}$$

The presence of non zero tensor Wtb form factors does not change this in practice.

Moreover, the anomalous form factors change the top quark decay width.

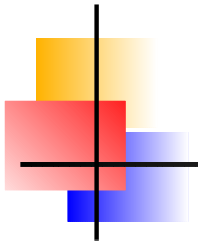

FBA in $t\bar{t}$ production at Tevatron

There are fluctuations in separate bins $\sim 1\sigma$, but integrated lowest order SM asymmetry is consistent with zero:

$$\begin{aligned} A_{t\bar{t}}^{\text{total}} &= -0.0013 \pm 0.0052, \\ A_{t\bar{t}}(m_{t\bar{t}} < 450\ \text{GeV}/c^2) &= 0.0009 \pm 0.0011 \\ A_{t\bar{t}}(m_{t\bar{t}} \geq 450\ \text{GeV}/c^2) &= -0.0027 \pm 0.0045. \end{aligned}$$

The presence of non zero tensor Wtb form factors does not change this in practice.

Moreover, the anomalous form factors change the top quark decay width. $\Rightarrow$ The prediction for top quark production rate is changed which is undesired, as it agrees well with the SM prediction.

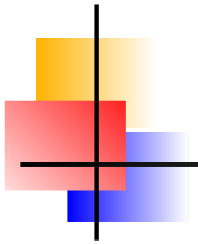

$t\bar{t}$ production at LHC

Consider the partonic sub-process of $p\bar{p} \to t\bar{t}$

$$gg \to bu\bar{d}\,\bar{b}\mu^{-}\bar{\nu}_{\mu}$$

taking into account the anomalous Wtb coupling. There are 421 Feynman diagrams, *in the unitary gauge, neglecting masses lighter than m_b and CKM mixing,* but much more complicated colour structure.

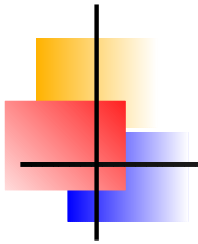

$t\bar{t}$ production at LHC

Consider the partonic sub-process of $p\bar{p} \to t\bar{t}$

$$gg \to bu\bar{d}\,\bar{b}\mu^-\bar{\nu}_\mu$$

taking into account the anomalous Wtb coupling. There are 421 Feynman diagrams, *in the unitary gauge, neglecting masses lighter than m_b and CKM mixing,* but much more complicated colour structure.

Cuts:

$$p_{Tl} > 30\,\mathrm{GeV}/c, \quad p_{Tj} > 30\,\mathrm{GeV}/c, \qquad |\eta_l| < 2.1, \quad |\eta_j| < 2.4,$$

$$\not{E}^T > 20\,\mathrm{GeV}, \qquad \Delta R_{ll,lj,jj} > 0.4.$$

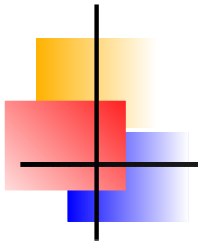

$t\bar{t}$ production at LHC

Consider the partonic sub-process of $p\bar{p} \to t\bar{t}$

$$gg \to bu\bar{d}\,\bar{b}\mu^-\bar{\nu}_\mu$$

taking into account the anomalous Wtb coupling. There are 421 Feynman diagrams, *in the unitary gauge, neglecting masses lighter than m_b and CKM mixing*, but much more complicated colour structure.

Cuts:

$$p_{Tl} > 30\,\mathrm{GeV}/c, \quad p_{Tj} > 30\,\mathrm{GeV}/c, \quad |\eta_l| < 2.1, \quad |\eta_j| < 2.4,$$

$$\not{E}^T > 20\,\mathrm{GeV}, \qquad \Delta R_{ll,lj,jj} > 0.4.$$

Scale choice: $Q = \sqrt{m_t^2 + \sum_j p_{Tj}^2}$.

$t\bar{t}$ production at LHC

Distributions in p_T [GeV/c] of the final state lepton. CP-even combinations of form factors.

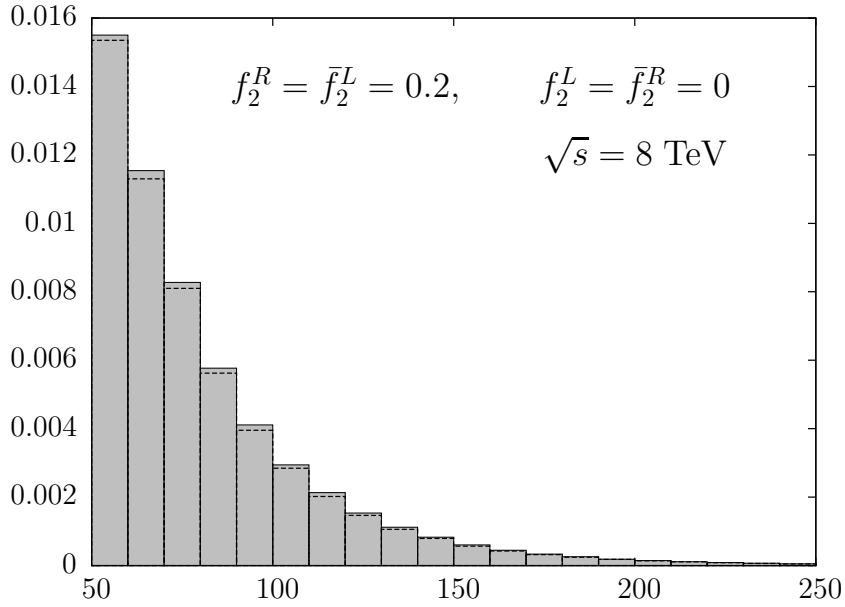

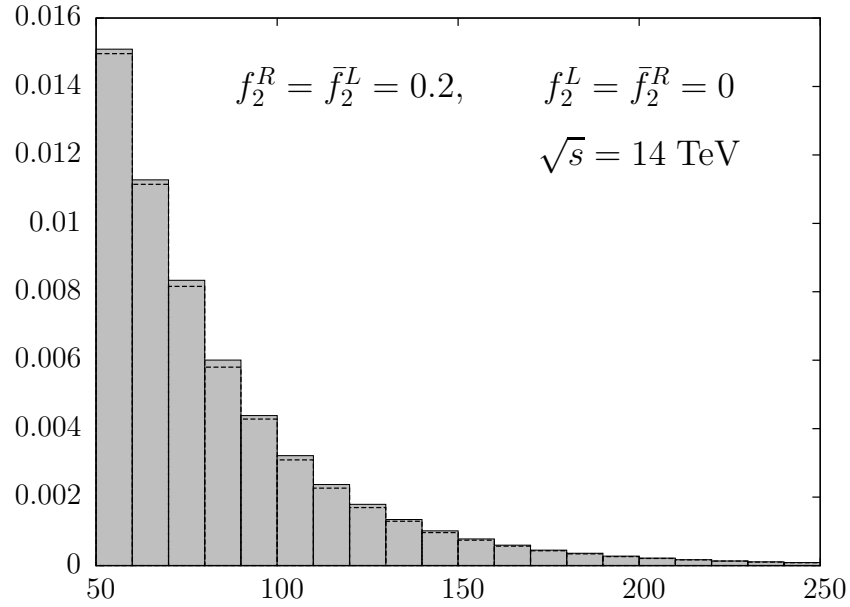

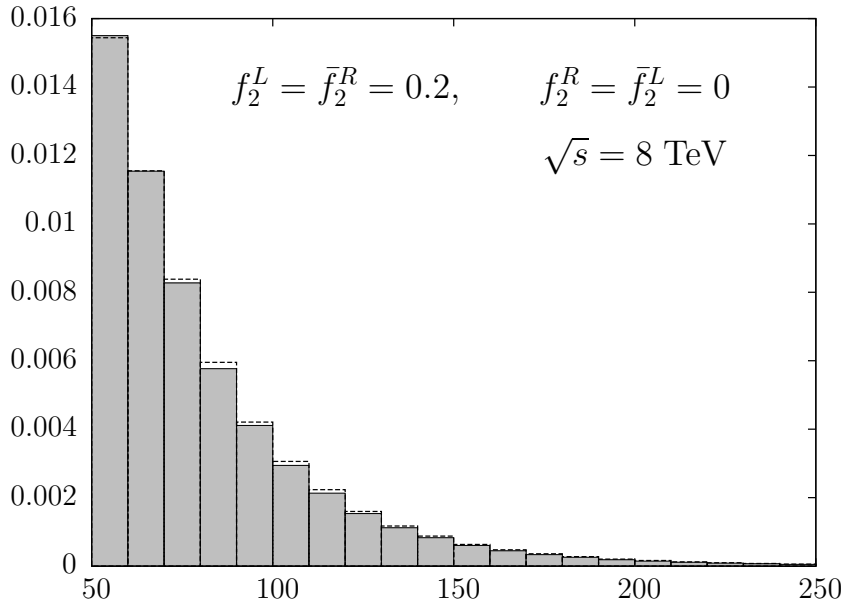

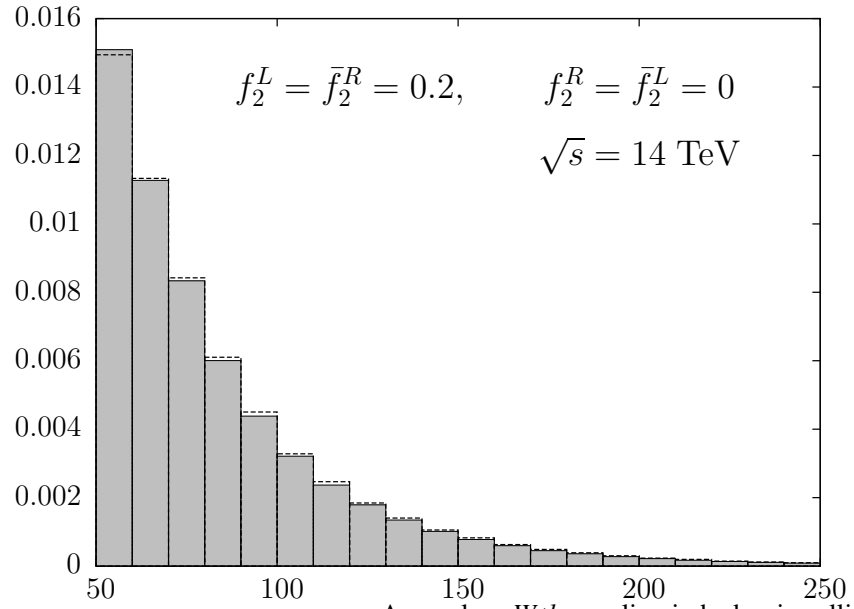

$t\bar{t}$ production at LHC

Distributions in p_T [GeV/c] of the final state lepton. CP-odd combinations of form factors.

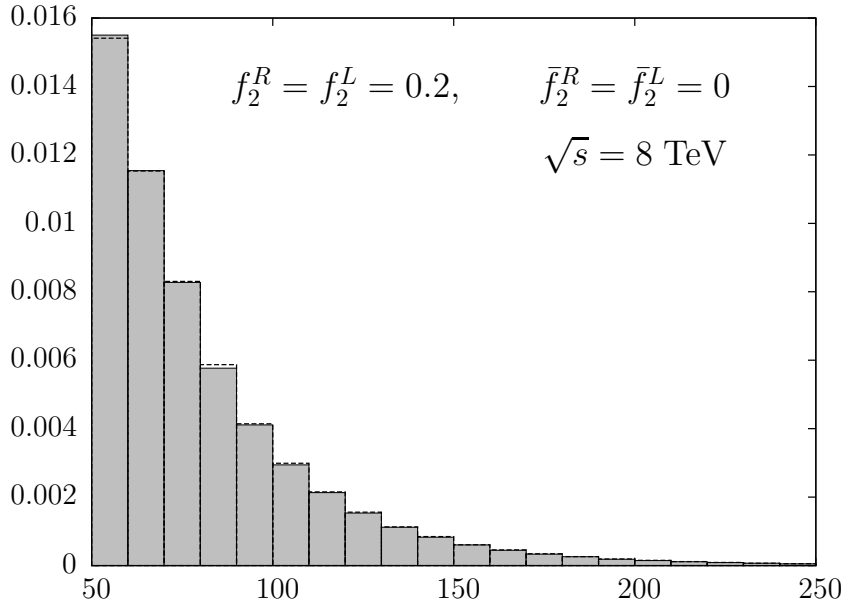

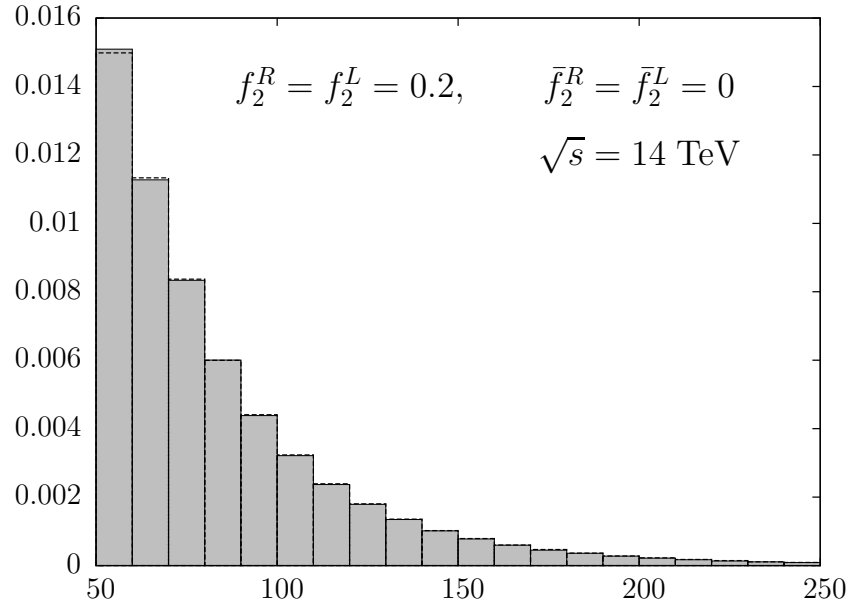

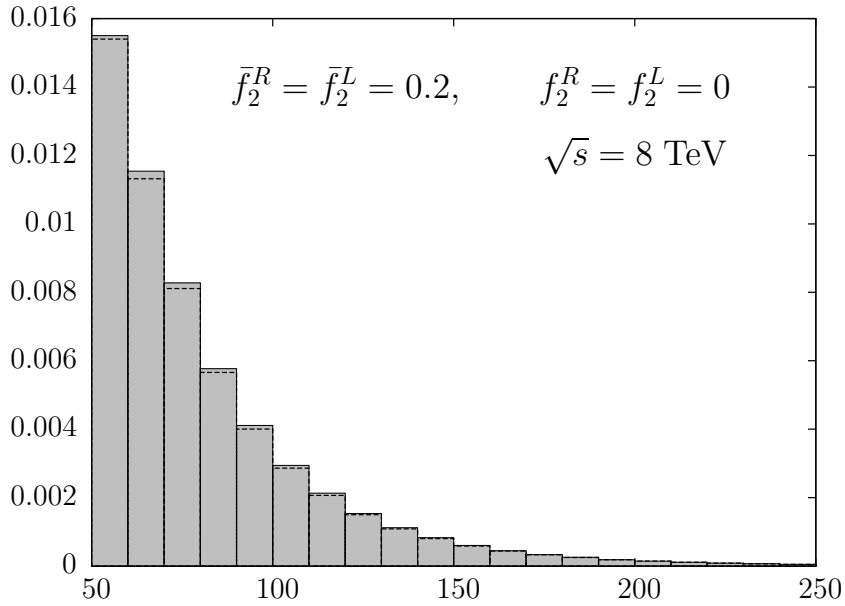

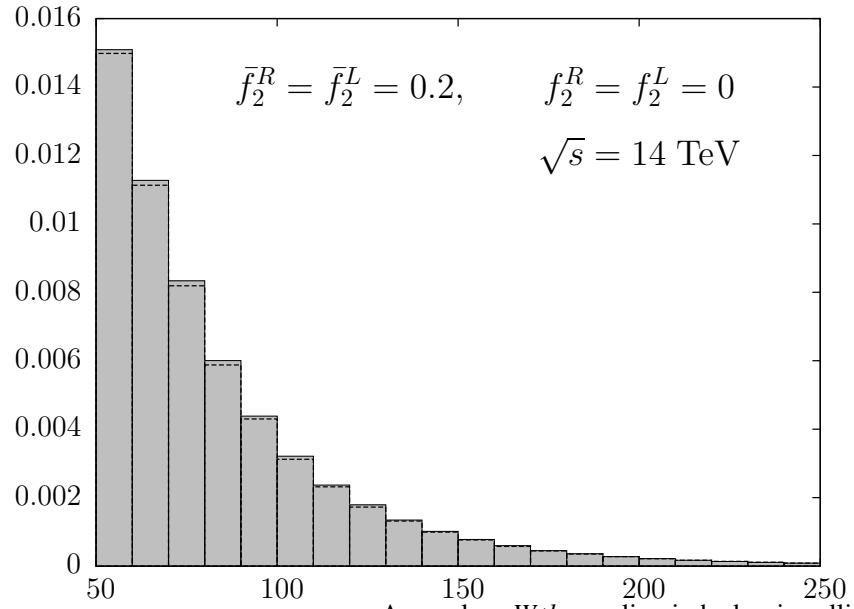

$t\bar{t}$ production at LHC

Distributions in $\cos\theta_{lt}$. CP-even combinations of form factors.

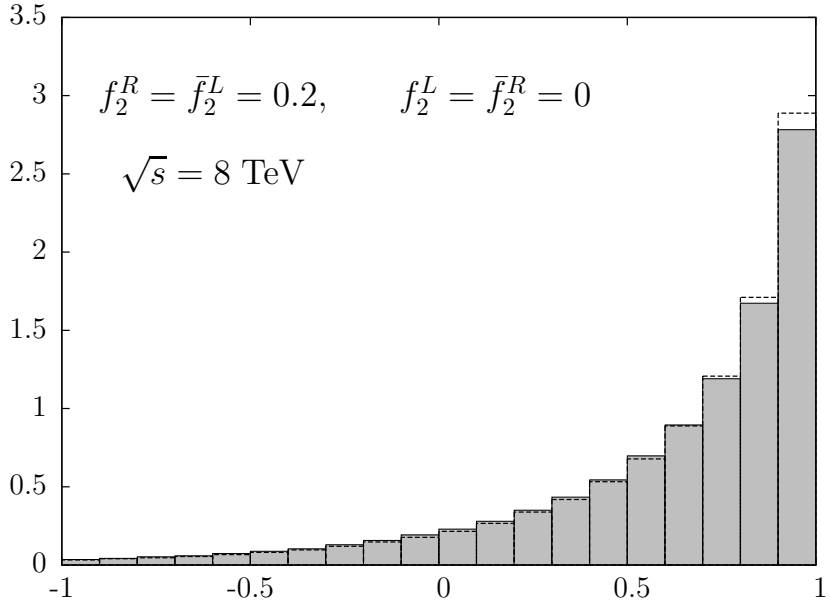

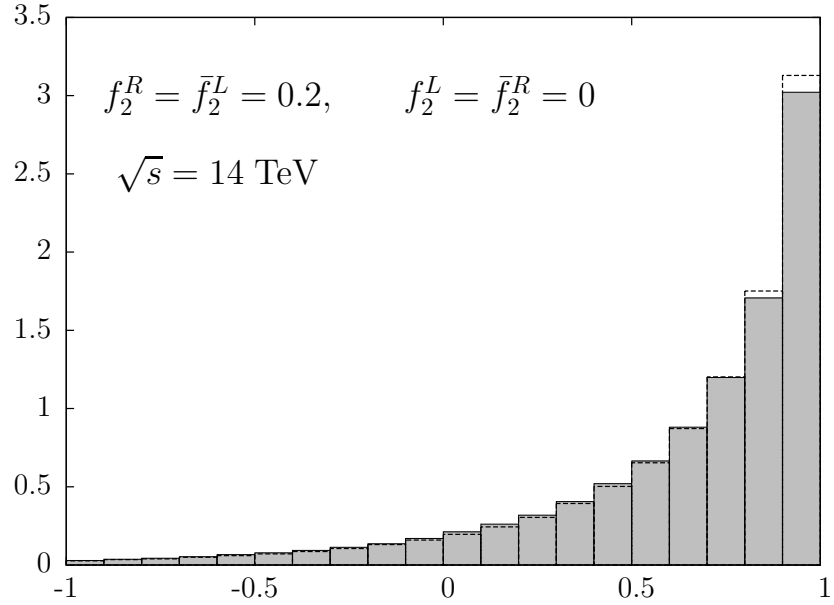

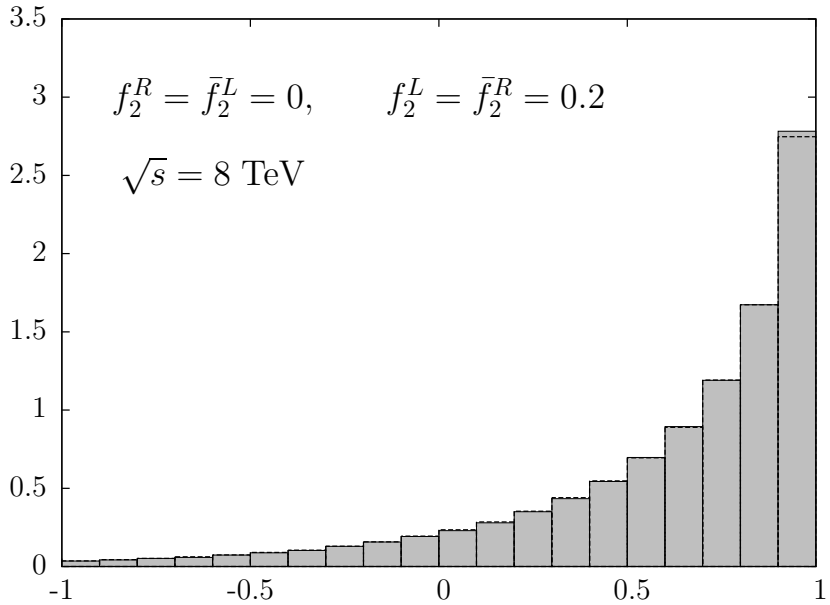

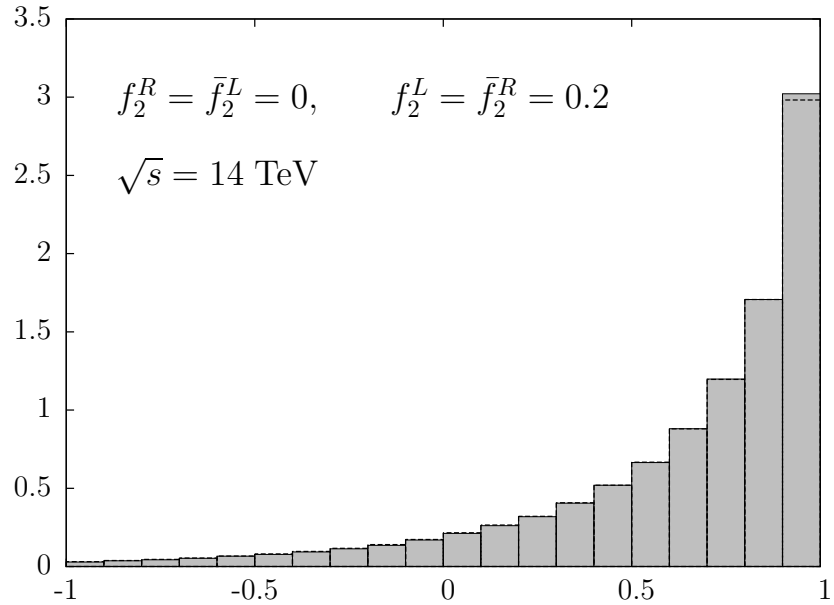

$t\bar{t}$ production at LHC

Distributions in $\cos\theta_{lt}$. CP-odd combinations of form factors.

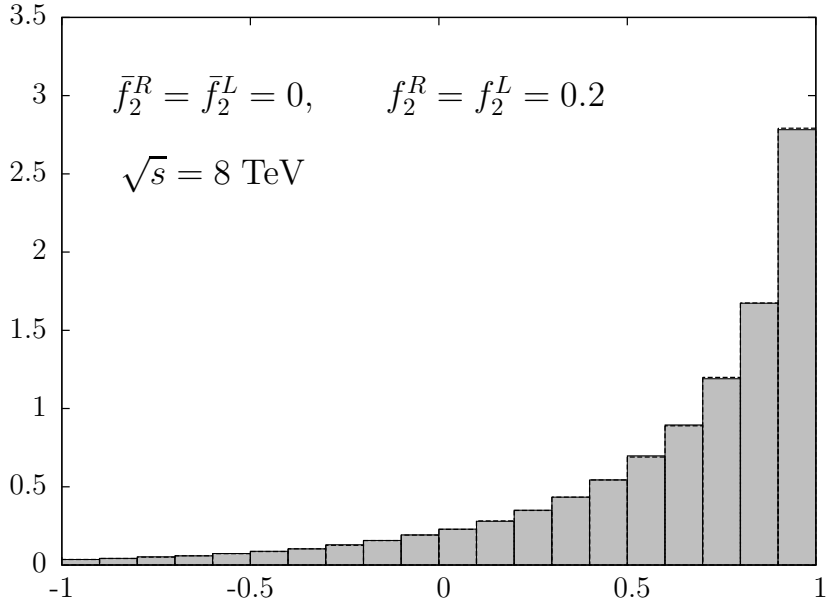

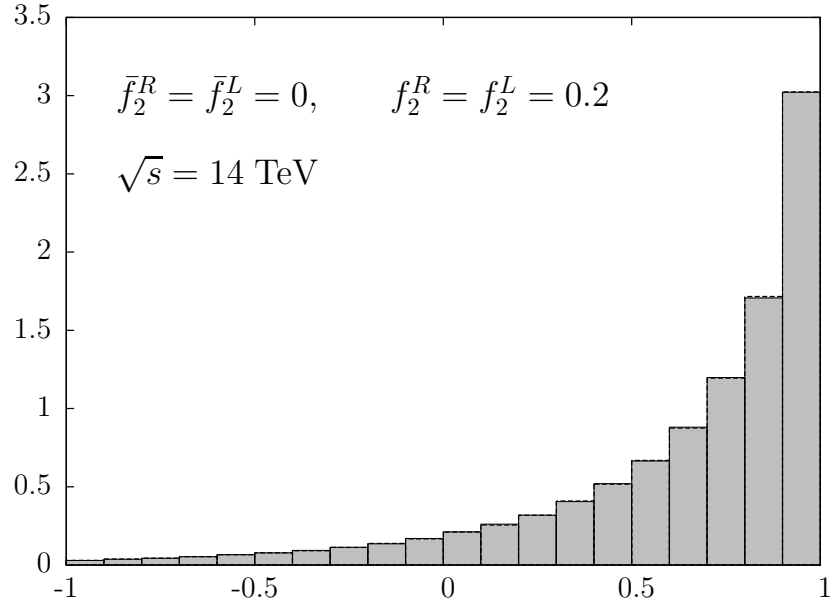

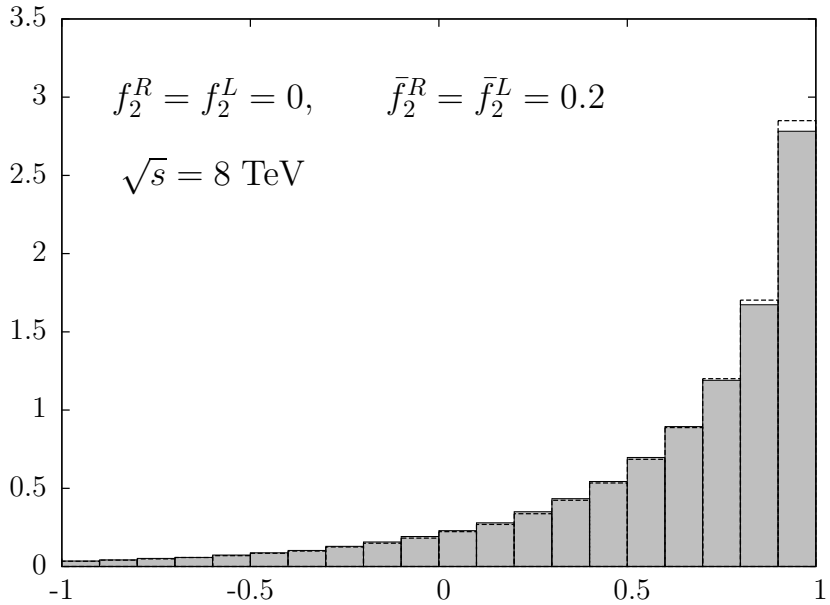

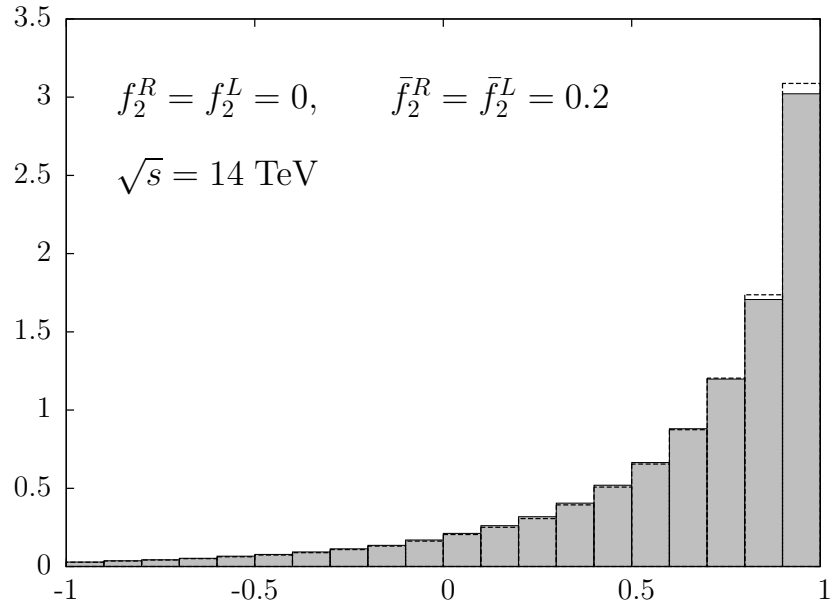

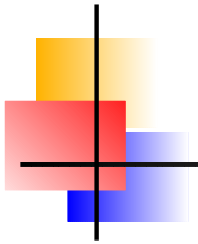

Summary and outlook

- The most general effective Lagrangian of the Wtb interaction containing operators of dimension four and five has been implemented in `carlomat`.

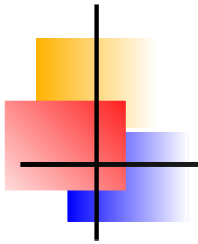

Summary and outlook

- The most general effective Lagrangian of the Wtb interaction containing operators of dimension four and five has been implemented in `carlomat`.
- The anomalous Wtb coupling does not explain the forward-backward asymmetry in the top quark pair production observed at the Tevatron.

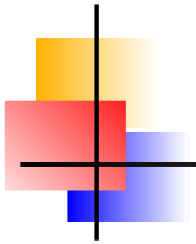

Summary and outlook

- The most general effective Lagrangian of the Wtb interaction containing operators of dimension four and five has been implemented in `carlomat`.
- The anomalous Wtb coupling does not explain the forward-backward asymmetry in the top quark pair production observed at the Tevatron.
- The effects of the anomalous Wtb coupling are hardly visible in differential distributions at the Tevatron and LHC energies, both in the CP-even CP-odd case.

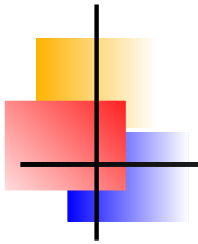

Summary and outlook

- The most general effective Lagrangian of the Wtb interaction containing operators of dimension four and five has been implemented in `carlomat`.
- The anomalous Wtb coupling does not explain the forward-backward asymmetry in the top quark pair production observed at the Tevatron.
- The effects of the anomalous Wtb coupling are hardly visible in differential distributions at the Tevatron and LHC energies, both in the CP-even CP-odd case.

Similar decoupling was found in the top quark pair production at the e^+e^- collisions [K. Kołodziej, Phys. Lett. **B584** (2004) 89].

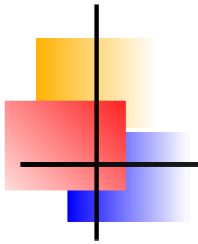

Summary and outlook

- The most general effective Lagrangian of the Wtb interaction containing operators of dimension four and five has been implemented in `carlomat`.
- The anomalous Wtb coupling does not explain the forward-backward asymmetry in the top quark pair production observed at the Tevatron.
- The effects of the anomalous Wtb coupling are hardly visible in differential distributions at the Tevatron and LHC energies, both in the CP-even CP-odd case.

Similar decoupling was found in the top quark pair production at the e^+e^- collisions [K. Kołodziej, Phys. Lett. **B584** (2004) 89].

New version of the program will be released, hopefully soon.

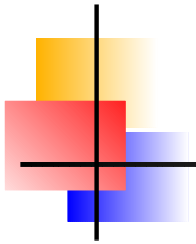

What `carlomat` *is?*

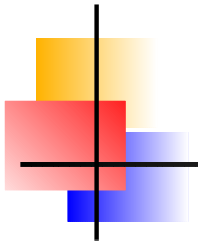

What `carlomat` *is?*

`carlomat` is a program for automatic computation of the lowest order cross sections,

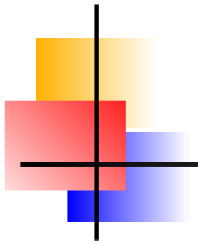

What `carlomat` *is?*

`carlomat` is a program for automatic computation of the lowest order cross sections, dedicated in particular for the description of multiparticle reactions of the form

$$p_1 + p_2 \to p_3 + \ldots + p_n$$

with the maximum of $n = 12$.

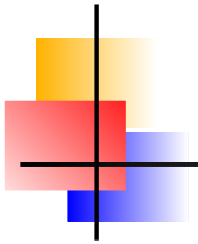

What carlomat *is?*

carlomat is a program for automatic computation of the lowest order cross sections, dedicated in particular for the description of multiparticle reactions of the form

$$p_1 + p_2 \to p_3 + \ldots + p_n$$

with the maximum of $n = 12$.

carlomat is written in Fortran 90/95.

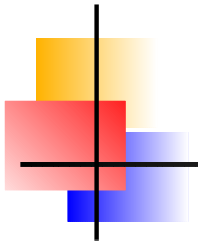

What `carlomat` *is?*

`carlomat` is a program for automatic computation of the lowest order cross sections, dedicated in particular for the description of multiparticle reactions of the form

$$p_1 + p_2 \to p_3 + \ldots + p_n$$

with the maximum of $n = 12$.

`carlomat` is written in Fortran 90/95.

It generates the matrix element for a user specified process together with phase space parametrizations which are used for the multichannel Monte Carlo integration of the lowest order cross sections and event generation.

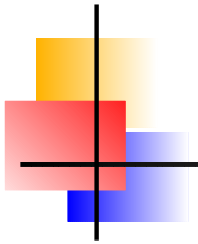

What `carlomat` *is?*

Version 1.0 was released 3 years ago:

- K. Kołodziej, Comput. Phys. Commun. 180 (2009) 1671.

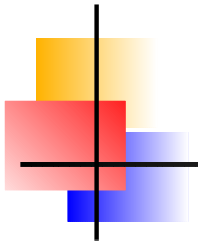

What `carlomat` *is?*

Version 1.0 was released 3 years ago:

- K. Kołodziej, Comput. Phys. Commun. 180 (2009) 1671.

Since then the program has been successfully used for calculating cross sections of many different reactions, as, e.g., all SM reactions of the form

$$e^+e^- \to b f_1 \bar{f}_1' \bar{b} f_2 \bar{f}_2' b \bar{b},$$

where $f_1, f_2' = \nu_e, \nu_\mu, \nu_\tau, u, c$ and $f_1', f_2 = e^-, \mu^-, \tau^-, d, s,$

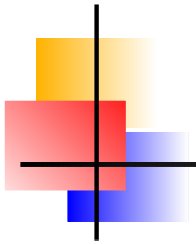

What `carlomat` *is?*

Version 1.0 was released 3 years ago:

- K. Kołodziej, Comput. Phys. Commun. 180 (2009) 1671.

Since then the program has been successfully used for calculating cross sections of many different reactions, as, e.g., all SM reactions of the form

$$e^+e^- \to b f_1 \bar{f}_1' \bar{b} f_2 \bar{f}_2' b \bar{b},$$

where $f_1, f_2' = \nu_e, \nu_\mu, \nu_\tau, u, c$ and $f_1', f_2 = e^-, \mu^-, \tau^-, d, s$, that are relevant for the associated production an decay of a top quark pair and a light Higgs boson at the e^+e^- linear collider.

- K. K., S. Szczypiński, Nucl. Phys. B801 (2008) 153 and Eur. Phys. J. C64 (2009) 645.

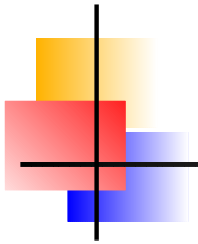

Use of `carlomat`

There are 240 966 Feynman diagrams for the hadronic channel

$$e^+e^- \to bc\bar{s}\bar{b}s\bar{c}b\bar{b},$$

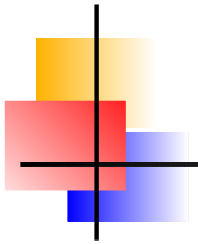

Use of `carlomat`

There are 240 966 Feynman diagrams for the hadronic channel

$$e^+e^- \to bc\bar{s}\bar{b}s\bar{c}b\bar{b},$$

(unitary gauge, $m_e = m_s = 0$, no CKM mixing.)

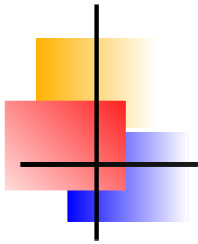

Use of `carlomat`

There are 240 966 Feynman diagrams for the hadronic channel

$$e^+e^- \to bc\bar{s}\bar{b}s\bar{c}b\bar{b},$$

(unitary gauge, $m_e = m_s = 0$, no CKM mixing.)

The matrix element M, which is calculated in the helicity base, is rather complicated.

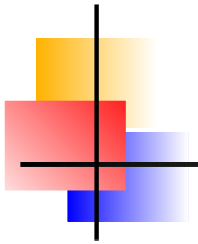

Use of `carlomat`

There are 240 966 Feynman diagrams for the hadronic channel

$$e^+e^- \to bc\bar{s}\bar{b}s\bar{c}b\bar{b},$$

(unitary gauge, $m_e = m_s = 0$, no CKM mixing.)

The matrix element M, which is calculated in the helicity base, is rather complicated. However, if the Monte Carlo summing over helicities is applied, calculating $\overline{|M|^2}$ is not a problem in practice.

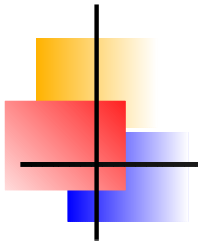

Use of `carlomat`

There are 240 966 Feynman diagrams for the hadronic channel

$$e^+e^- \to bc\bar{s}\bar{b}s\bar{c}b\bar{b},$$

(unitary gauge, $m_e = m_s = 0$, no CKM mixing.)
The matrix element M, which is calculated in the helicity base, is rather complicated. However, if the Monte Carlo summing over helicities is applied, calculating $\overline{|M|^2}$ is not a problem in practice.
The main issue is to calculate the integral over

$$8 \times 3 - 4 = 20$$

dimensional phase space.

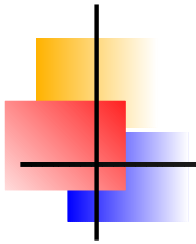

Phase space integration

Final state particles $\{p_3, p_4, \ldots, p_n\}$ are divided into two subsets of four momenta q_{i_1} and q_{i_2}, defined in the relative c.m.s.

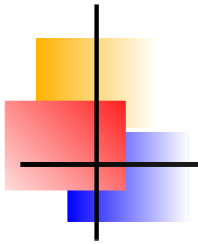

Phase space integration

Final state particles $\{p_3, p_4, \ldots, p_n\}$ are divided into two subsets of four momenta q_{i_1} and q_{i_2}, defined in the relative c.m.s.

This is done in a way that depends on a topology of the diagram.

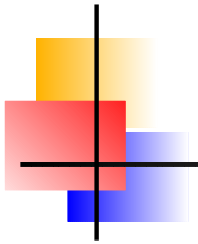

Phase space integration

Final state particles $\{p_3, p_4, \ldots, p_n\}$ are divided into two subsets of four momenta q_{i_1} and q_{i_2}, defined in the relative c.m.s.

This is done in a way that depends on a topology of the diagram.

Using consecutively the identity

$$\int \mathrm{d}s_i \int \frac{\mathrm{d}^3 q_i}{2E_i}\, \delta^{(4)}\left(q_i - q_{i_1} - q_{i_2}\right) = 1, \qquad E_i^2 = s_i + \vec{q}_i^{\,2}$$

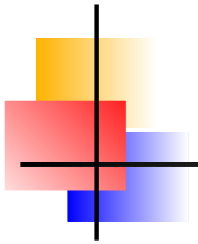

Phase space integration

Final state particles $\{p_3, p_4, \ldots, p_n\}$ are divided into two subsets of four momenta q_{i_1} and q_{i_2}, defined in the relative c.m.s.

This is done in a way that depends on a topology of the diagram.

Using consecutively the identity

$$\int \mathrm{d}s_i \int \frac{\mathrm{d}^3 q_i}{2E_i}\, \delta^{(4)}\left(q_i - q_{i_1} - q_{i_2}\right) = 1, \qquad E_i^2 = s_i + \vec{q}_i^{\,2}$$

the phase space element

$$\mathrm{d}^{3n_f-4}Lips = (2\pi)^4 \delta^{(4)}\left(p_1 + p_2 - \sum_{i=3}^{n} p_i\right) \prod_{i=3}^{n} \frac{\mathrm{d}p_i^3}{(2\pi)^3 2E_i},$$

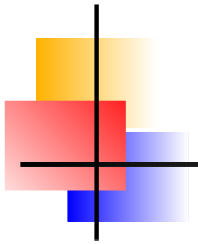

Phase space integration

Final state particles $\{p_3, p_4, \ldots, p_n\}$ are divided into two subsets of four momenta q_{i_1} and q_{i_2}, defined in the relative c.m.s.
This is done in a way that depends on a topology of the diagram.
Using consecutively the identity

$$\int \mathrm{d}s_i \int \frac{\mathrm{d}^3 q_i}{2E_i}\, \delta^{(4)}\left(q_i - q_{i_1} - q_{i_2}\right) = 1, \qquad E_i^2 = s_i + \vec{q}_i^{\,2}$$

the phase space element

$$\mathrm{d}^{3n_f-4}Lips = (2\pi)^4 \delta^{(4)}\left(p_1 + p_2 - \sum_{i=3}^{n} p_i\right) \prod_{i=3}^{n} \frac{\mathrm{d}p_i^3}{(2\pi)^3 2E_i},$$

is brought into the form

$$\mathrm{d}^{3n_f-4}Lips = (2\pi)^{4-3n_f}\, \mathrm{d}l_0 \mathrm{d}l_1 \ldots \mathrm{d}l_{n-4} \mathrm{d}s_1 \mathrm{d}s_2 \ldots \mathrm{d}s_{n-4}.$$

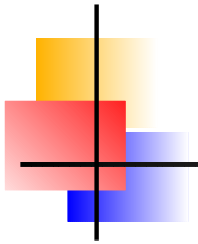

Phase space integration

In

$$\mathrm{d}^{3n_f-4}Lips = (2\pi)^{4-3n_f}\,\mathrm{d}l_0\mathrm{d}l_1\ldots\mathrm{d}l_{n-4}\mathrm{d}s_1\mathrm{d}s_2\ldots\mathrm{d}s_{n-4},$$

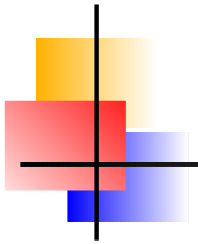

Phase space integration

In

$$\mathrm{d}^{3n_f-4}Lips = (2\pi)^{4-3n_f}\,\mathrm{d}l_0\mathrm{d}l_1\ldots\mathrm{d}l_{n-4}\mathrm{d}s_1\mathrm{d}s_2\ldots\mathrm{d}s_{n-4},$$

invariants s_i are given by

$$s_i = \begin{cases} (q_{i_1}+q_{i_2})^2 = (E_{i_1}+E_{i_2})^2, & \text{for } i = 1,\ldots,n-4 \\ (p_1+p_2)^2 = s, & \text{for } i = 0 \end{cases}$$

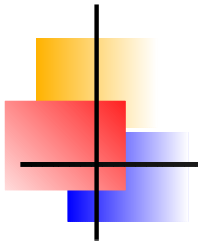

Phase space integration

In

$$\mathrm{d}^{3n_f-4}Lips = (2\pi)^{4-3n_f}\,\mathrm{d}l_0\mathrm{d}l_1\ldots\mathrm{d}l_{n-4}\mathrm{d}s_1\mathrm{d}s_2\ldots\mathrm{d}s_{n-4},$$

invariants s_i are given by

$$s_i = \begin{cases} (q_{i_1}+q_{i_2})^2 = (E_{i_1}+E_{i_2})^2, & \text{for } i = 1,\ldots,n-4 \\ (p_1+p_2)^2 = s, & \text{for } i = 0 \end{cases}$$

and the two particle phase space elements $\mathrm{d}l_i$ are given by

$$\mathrm{d}l_i = \frac{\lambda^{\frac{1}{2}}\left(s_i, q_{i_1}^2, q_{i_2}^2\right)}{2\sqrt{s_i}}\mathrm{d}\Omega_i,$$

where λ is the kinematical function, Ω_i is the solid angle of momentum $\vec{q}_{i_1}$ in the relative c.m.s., $\vec{q}_{i_1}+\vec{q}_{i_2} = \vec{0}$.

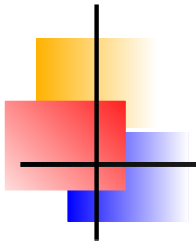

Phase space integration

Invariants s_i are randomly generated within their physical limits, $s_i^{\min}$ and $s_i^{\max}$,

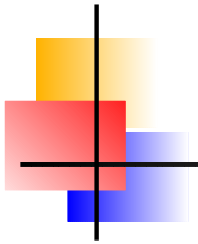

Phase space integration

Invariants s_i are randomly generated within their physical limits, $s_i^{\min}$ and $s_i^{\max}$, which are deduced from a topology of the Feynman diagram.

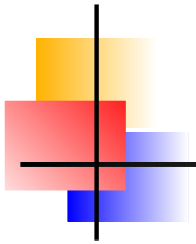

Phase space integration

Invariants s_i are randomly generated within their physical limits, $s_i^{\min}$ and $s_i^{\max}$, which are deduced from a topology of the Feynman diagram.

They are generated either according to the uniform distribution

or,

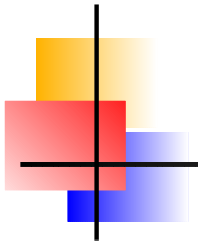

Phase space integration

Invariants s_i are randomly generated within their physical limits, $s_i^{\min}$ and $s_i^{\max}$, which are deduced from a topology of the Feynman diagram.

They are generated either according to the uniform distribution or, if necessary, mappings of the Breit-Wigner shape of the propagators of unstable particles and $\sim 1/s$ behaviour of the propagators of mass-less particles are performed.

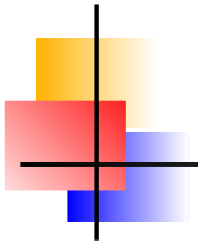

Phase space integration

Invariants s_i are randomly generated within their physical limits, $s_i^{\min}$ and $s_i^{\max}$, which are deduced from a topology of the Feynman diagram.

They are generated either according to the uniform distribution or, if necessary, mappings of the Breit-Wigner shape of the propagators of unstable particles and $\sim 1/s$ behaviour of the propagators of mass-less particles are performed.

An option is included in the program that allows to turn on the mapping if the particle decays into 2, 3, 4, ... on-shell particles.

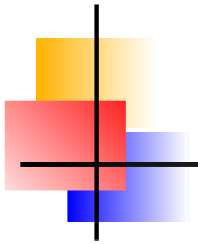

Phase space integration

Invariants s_i are randomly generated within their physical limits, $s_i^{\min}$ and $s_i^{\max}$, which are deduced from a topology of the Feynman diagram.

They are generated either according to the uniform distribution or, if necessary, mappings of the Breit-Wigner shape of the propagators of unstable particles and $\sim 1/s$ behaviour of the propagators of mass-less particles are performed.

An option is included in the program that allows to turn on the mapping if the particle decays into 2, 3, 4, ... on-shell particles.

Different phase space parametrizations obtained in this way can be used for testing purposes.

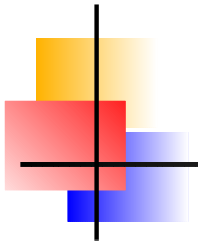

Phase space integration

In `carlomat` v. 1.0, the phase space parametrization is generated for each of N Feynman diagrams of the considered process

$$f_i(x) = \mathrm{d}^{3n_f-4} Lips_i(x) \qquad i = 1, \ldots, N,$$

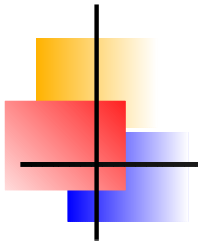

Phase space integration

In `carlomat` v. 1.0, the phase space parametrization is generated for each of N Feynman diagrams of the considered process

$$f_i(x) = \mathrm{d}^{3n_f-4} Lips_i(x) \qquad i = 1,\ldots,N,$$

where $x = \left(x_1,\ldots,x_{3n_f-4}\right)$ are uniformly distributed random arguments and the normalization condition

$$\int_0^1 \mathrm{d}x^{3n_f-4} f_i(x) = \mathrm{vol}(Lips)$$

is satisfied for each parametrization.

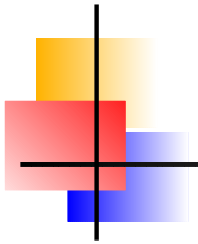

Phase space integration

All the parametrizations $f_i(x)$ are then automatically combined into a single multichannel probability distribution

$$f(x) = \sum_{i=1}^{N} a_i f_i(x),$$

with non negative weights a_i, $i = 1, \ldots, N$,

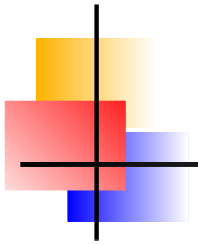

Phase space integration

All the parametrizations $f_i(x)$ are then automatically combined into a single multichannel probability distribution

$$f(x) = \sum_{i=1}^{N} a_i f_i(x),$$

with non negative weights a_i, $i = 1, \ldots, N$, satisfying the condition

$$\sum_{i=1}^{N} a_i = 1 \qquad \Leftrightarrow \qquad \int_0^1 \mathrm{d}x^{3n_f-4} f(x) = \mathrm{vol}(Lips).$$

Phase space integration

All the parametrizations $f_i(x)$ are then automatically combined into a single multichannel probability distribution

$$f(x) = \sum_{i=1}^{N} a_i f_i(x),$$

with non negative weights a_i, $i = 1, \ldots, N$, satisfying the condition

$$\sum_{i=1}^{N} a_i = 1 \qquad \Leftrightarrow \qquad \int_0^1 \mathrm{d}x^{3n_f-4} f(x) = \mathrm{vol}(Lips).$$

The actual MC integration is done with the random numbers generated according to probability distribution $f(x)$.

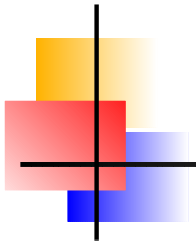

Phase space integration

Integration in `carlomat` can be performed iteratively.

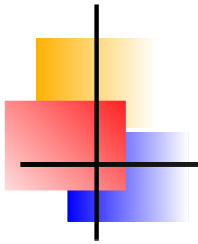

Phase space integration

Integration in `carlomat` can be performed iteratively.

First, the MC integral is calculated N times with a rather small number of calls to the integrand,

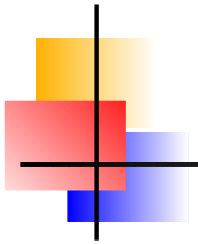

Phase space integration

Integration in `carlomat` can be performed iteratively.

First, the MC integral is calculated N times with a rather small number of calls to the integrand, each time with a different phase space parametrization $f_i(x)$.

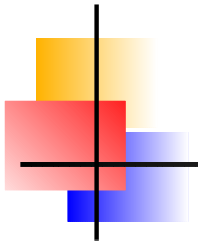

Phase space integration

Integration in `carlomat` can be performed iteratively.

First, the MC integral is calculated N times with a rather small number of calls to the integrand, each time with a different phase space parametrization $f_i(x)$.

The result σ_i obtained with the i-th parametrization is used to calculate new weights according to the following formula

$$a_i = \sigma_i / \sum_{j=1}^{N} \sigma_j .$$

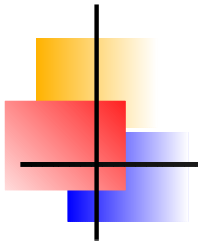

Phase space integration

Integration in `carlomat` can be performed iteratively.

First, the MC integral is calculated N times with a rather small number of calls to the integrand, each time with a different phase space parametrization $f_i(x)$.

The result σ_i obtained with the i-th parametrization is used to calculate new weights according to the following formula

$$a_i = \sigma_i / \sum_{j=1}^{N} \sigma_j .$$

This is the probability of choosing i-th parametrization in the first iteration.

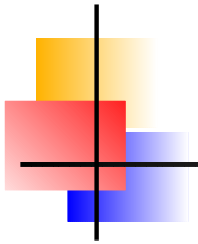

Phase space integration

Integration in `carlomat` can be performed iteratively.

First, the MC integral is calculated N times with a rather small number of calls to the integrand, each time with a different phase space parametrization $f_i(x)$.

The result σ_i obtained with the i-th parametrization is used to calculate new weights according to the following formula

$$a_i = \sigma_i / \sum_{j=1}^{N} \sigma_j .$$

This is the probability of choosing i-th parametrization in the first iteration. $\Rightarrow$ Channels with small weights a_i are not chosen and will have zero weights in the next iteration.

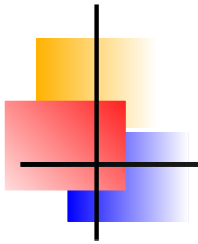

Phase space integration

After the first iteration has been completed, the new weights for the second iteration can be determined analogously

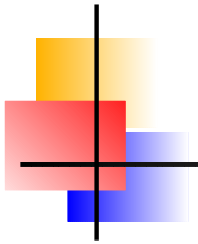

Phase space integration

After the first iteration has been completed, the new weights for the second iteration can be determined analogously and so on.

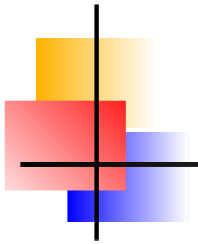

Phase space integration

After the first iteration has been completed, the new weights for the second iteration can be determined analogously and so on. After several iterations only the most important kinematical channels survive.

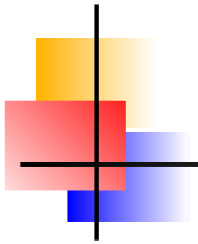

Phase space integration

After the first iteration has been completed, the new weights for the second iteration can be determined analogously and so on.
After several iterations only the most important kinematical channels survive.
Large number of kinematical channels in the beginning $\Rightarrow$ very long compilation time.

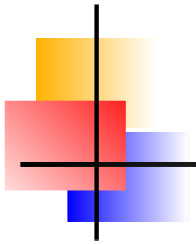

Phase space integration

Improvements in the current version of `carlomat`:

- Commands for calculating phase space boundaries and boosts of four momenta to the c.m.s. are generated only once for all parametrizations corresponding to diagrams of the same topology.

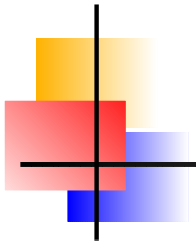

Phase space integration

Improvements in the current version of `carlomat`:

- Commands for calculating phase space boundaries and boosts of four momenta to the c.m.s. are generated only once for all parametrizations corresponding to diagrams of the same topology.
- Kinematical routines corresponding to diagrams of the same topology that contain the same mappings are discarded at the stage of code generation.

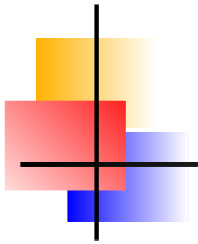

Phase space integration

Improvements in the current version of `carlomat`:

- Commands for calculating phase space boundaries and boosts of four momenta to the c.m.s. are generated only once for all parametrizations corresponding to diagrams of the same topology.
- Kinematical routines corresponding to diagrams of the same topology that contain the same mappings are discarded at the stage of code generation.

$\Rightarrow$ Reduction of a compilation time, typically by a factor $2-5$ for multiparticle processes, is achieved.